Proc. Natl. Acad. Sci. USA
Vol. 74, No. 8, pp. 3370–3374, August 1977
Biophysics

Microtubule structure at low resolution by x-ray diffraction

(tubulin/helical diffraction)

ECKHARD MANDELKOW*, JOSEPH THOMAS†, AND CAROLYN COHEN†‡

* Max-Planck-Institut für medizinische Forschung, D-69 Heidelberg, Jahnstrasse 29, West Germany; and † Rosenstiel Basic Medical Sciences Research Center, Brandeis University, Waltham, Massachusetts 02154

Communicated by Frederick M. Richards, May 13, 1977

ABSTRACT **Analysis of x-ray diagrams of oriented hydrated cytoplasmic microtubules shows that the tubule wall extends from about 70 to 150 Å radially. The central region of the wall appears homogeneous, but the outside surface is subdivided by vertical grooves separating the 13 protofilaments and by a steep 10-fold family of grooves. The inside surface is dominated by the 10-start grooves with no clear subdivision between the protofilaments.**

We have recently prepared well-oriented gels of calf brain microtubules that give detailed x-ray diffraction patterns (1). The most prominent feature of the diagrams is a series of reflections on layer lines indicating a 40 Å axial repeat, with strong diffraction out to spacings of about 10 Å (Fig. 1). In order to interpret the x-ray results, we make use of certain features of the microtubule as imaged in the electron microscope (Fig. 2). By combining the x-ray data with this information, we have produced a low-resolution (25 Å) three-dimensional model for the hydrated microtubule which reveals new aspects of the structure.

The main component of microtubules is the protein tubulin (55,000 daltons), which associates strongly into a heterodimer (10) composed of α- and β-tubulin monomers that are chemically very similar (3, 12). Brain tubulin readily polymerizes into microtubules with a rise in temperature, and the microtubules are stabilized by reagents such as glycerol (3, 4). To prepare x-ray specimens, microtubules are centrifuged to form birefringent gels and are oriented with the long axis of the particles parallel to the axis of the quartz capillary. The x-ray beam is perpendicular to the particles, and, because there appears to be little evidence of interparticle interference effects, the diagrams record the cylindrically averaged diffraction from a single microtubule.

The strategy used in the analysis of the x-ray diagram is that outlined by Cohen *et al.* (1); i.e., we interpret the pattern on the basis of a single diffracting system. The first step in the structure determination is the analysis of the equatorial diffraction near the origin; this gives the boundaries of the microtubule wall. A reliable estimate of wall thickness is needed to interpret the diffraction maxima on the other layer lines. With this information, we can construct a model showing the distribution of mass of the microtubule wall.

Analysis of equator

The first three subsidiary maxima of the equatorial intensity (Fig. 3A) are characteristic of diffraction from a thick-walled cylindrical shell (1, 13). The mean radius is about 110 Å, and the inner and outer radii are about 70 Å and 150 Å, respectively; note that the ratio of the inner to outer radius is about one-half. The equatorial peak at 53 Å (Fig. 3*A*; $R = 0.0188$ Å^{-1}) would not arise from a uniform tubule wall but, rather, from the subdivision of the wall into longitudinal filaments ("protofilaments"). Electron micrographs show that the microtubule is made up of 13 protofilaments (7, 8). The 53-Å reflection corresponds to the spacing between the 13 protofilaments along the outer wall of the cylinder at a radius of about 126 Å. One major difference is that the tubules seen by x-rays have a substantially greater outer diameter (300 Å) compared with the value of 240 Å generally taken from electron microscopy.

Apart from some weak subsidiary maxima, the next strong peak on the equator is at a spacing of 26 Å (Fig. 3*A*; $R = 0.0390$ Å^{-1}). This reflection could be interpreted as corresponding to a subdivision between 13 protofilaments on the inner surface of the wall located at a radius of 60 Å. However, this would place mass outside the wall dimensions determined above, so that we exclude this possibility. The alternative interpretation is that this peak corresponds to a 26-fold density fluctuation at about a radius of 115 Å in the particle wall. In principle, this fluctuation could be added at any angular position (phase) with respect to the protofilament. Phases are often obtained by labeling the protein with heavy atoms, but at low resolution one can use the phases calculated from electron micrographs. From such an analysis (see end of next section) the most plausible position for the 26-fold fluctuation would be roughly at the same angular origin as the 13-fold fluctuation. This interpretation suggests that deep grooves exist between the protofilaments and that each protofilament is split slightly (Fig. 4 *A* and *B*).

Analysis of the first layer line

The first layer line is characterized by four reflections, which appear on each side of the meridian. The first two, near the meridian, are weak; the second two, well away from the meridian, are strong (Figs. 1 and 3*B*). A noteworthy feature of each pair of reflections is that their distance from the meridian is in about the same ratio (i.e., 1/2) as that of the inner and outer radii of the tubule wall. This distribution of x-ray intensity can be simply interpreted on the basis of diffraction from the two surfaces of the tubule. each reflection can be thought of as coming from a small grating that reflects x-rays at right angles to its planes. Because the protein subunits extend from the inner to the outer wall of the tubule, the gratings described by the subunits on the inside have a steeper slope than the corresponding gratings on the outside. The pair of strong reflections thus shows that the wall is carved up by a fairly steep family of helices running at an angle of about 60° to the fiber axis on the outside of the particle, and 45° on the inside. Similarly, the weak pair of reflections near the center of the pattern on this

The costs of publication of this article were defrayed in part by the payment of page charges from funds made available to support the research which is the subject of the article. This article must therefore be hereby marked "advertisement" in accordance with 18 U. S. C. §1734 solely to indicate this fact.

‡ To whom requests for reprints should be addressed.

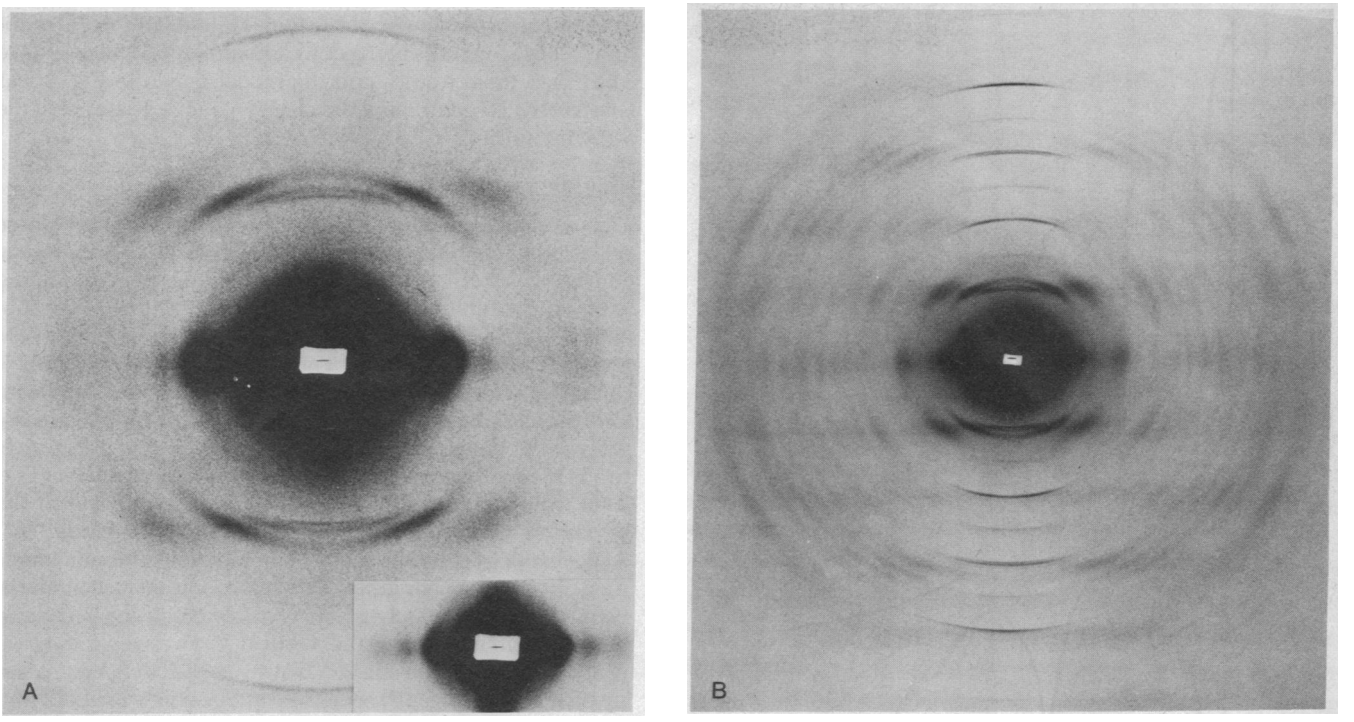

FIG. 1. X-ray diffraction patterns from an oriented gel of calf brain microtubules. The reflections lie on strong horizontal layer lines with an axial repeat of 40.5 Å. *A* and *B* (reproduced at different magnifications) extend to axial resolutions of 20 Å and 8 Å, respectively. The central scattering obscures the innermost reflections on the equator, which can be seen on weaker exposures (*A, inset*). The particle axes are disoriented from their mean (vertical) direction by a few degrees. As a result, reflections appear arced; thus, the two weak reflections that appear to be meridional on the first layer line are in fact four peaks, a pair on each side of the meridian (Fig. 3*B*). Tubulin was purifed (3, 4) using 0.075 M 2-(*N*-morpholino)ethanesulfonic acid (Mes), 1 mM ethylene glycol bis(β-aminoethyl ether)-*N,N'*-tetraacetic acid (EGTA), 1 mM GTP, 0.5–1.0 mM $MgCl_2$, at pH 6.5, with 0.1 mM dithiothreitol, 10^{-3}% sulfadiazine, and 25% vol/vol glycerol for polymerization. High-molecular-weight material, which makes up about 10% of the protein, copurifies with the tubulin. Other minor proteins are present in quantities amounting to roughly 5% of the total protein. The suspension of microtubules was centrifuged 24 hr at 97,000 × *g*, 32°C, to produce a birefringent pellet. The pelleted material (with microtubules oriented by centrifugation) was inserted into 1-mm quartz capillaries and sealed with buffer. The x-ray photographs were taken at room temperature on an Elliot GX-6 rotating anode with a quartz crystal focusing monochromator.

layer line arises from a set of shallow grooves on both the particle surfaces at a slight inclination (about 80° from the fiber axis). At this resolution, then, the x-ray pattern shows the particle wall to be grooved on both sides, particularly on the outside surface. The shape of the subunits produces marked channels following steep helices on the outside and inside (Fig. 4).

This grooving of the microtubule wall was qualitatively deduced by Cohen *et al.* (13) in 1971, but a rigorous interpretation requires more recent electron microscope results. Amos and Klug (5) showed the arrangement of protein subunits in the wall of negatively stained flagellar microtubules, and Erickson (6) confirmed their results for cytoplasmic microtubules. The basic

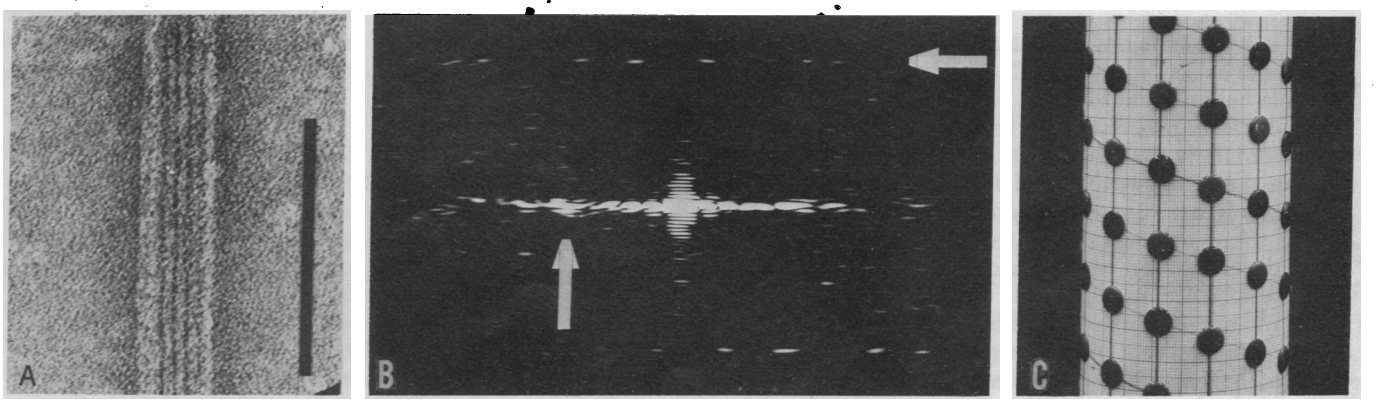

FIG. 2. (*A*) Electron micrograph of brain microtubules negatively stained with 1% uranyl acetate. The longitudinal protofilaments are clearly resolved as faint white lines, separated by about 50 Å. The bright edges come from the superposition of several protofilaments in projection. The bar length is 1000 Å.

(*B*) Optical diffraction pattern, revealing the 50-Å equatorial and 40-Å axial periodicity (arrows, see *text*).

(*C*) The array of subunits determined by electron microscopy of microtubules (5, 6). The subunits are arranged along helical lines (or families of helices). The intersections of the two sets of lines in the diagram define the symmetry (surface lattice) of the tubule and a unit cell given by four adjacent points. There are 13 vertical rows (7, 8) with a relative axial displacement of 9.2 Å. This defines a 3-start helix (connected by faint lines). Other helical families are generated by connecting the subunits in different directions. Thus, the diagonal of the unit cell defines the direction of a steep 10-start helical family. The 3-start helix is left-handed, the 10-start helix is right-handed (9).

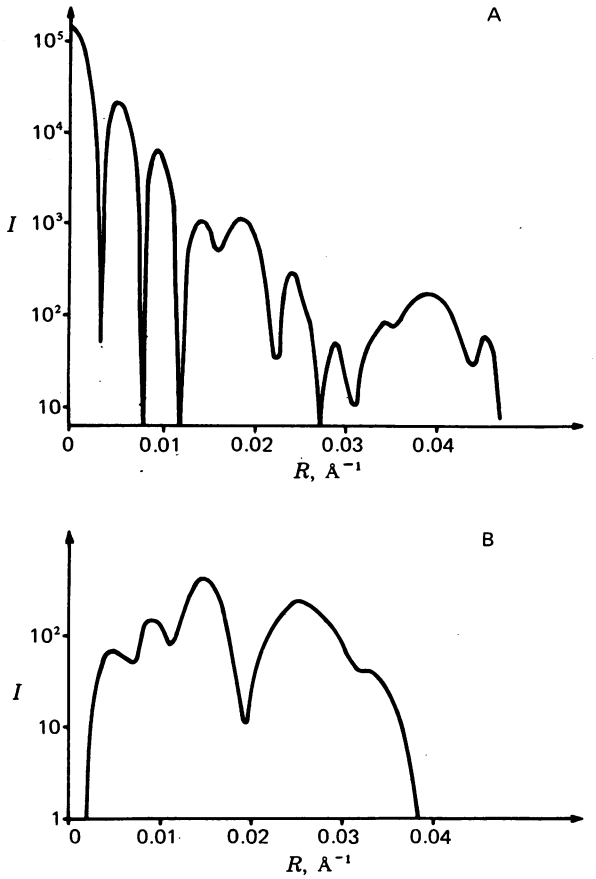

FIG. 3. Logarithmic plot of intensities versus $R = 2 \sin \theta/\lambda$.
(*A*) Equator. The first four peaks correspond to the diffraction from a uniform cylindrical shell. Peaks from $R = 0.0188$ Å^{-1} on belong to a 13-fold density fluctuation; the peak at $R = 0.0390$ Å^{-1} is from a 26-fold density fluctuation.
(*B*) The first layer line. The first two weak peaks ($R = 0.0045$ Å^{-1} and 0.0093 Å^{-1}) arise from the shallow 3-start helical grooves; the next two strong peaks ($R = 0.0145$ Å^{-1} and 0.0255 Å^{-1}) are from the deep 10-start grooves. Films were scanned on an Optronics densitometer with a 25-μm raster. Intensities were integrated along arcs using a program written by L. Makowski (2). Note difference between *A* and *B* in magnitudes of the peaks.

array is 13 protofilaments, each shifted axially by about 9 Å relative to its neighbor (Fig. 2*C*). This geometry specifies the possible helical families in the microtubule wall; i.e., all the subunits can be connected by 3 helices of low inclination or by a steeper family of 10 helices, etc. Thus, on the first layer line, the position of the weak pair of diffraction maxima (Fig. 3*B*) corresponds to the 3-start family of helices (Fig. 2*C*), while the pair of strong reflections comes from the steep 10-start helices. An independent test of these assignments is that the helical families specified must lie within the limits of the microtubule wall. This can readily be checked by our previous determination of the wall thickness from the equatorial diffraction. It turns out that the first pair of weak reflections can arise only from the 3-start helical grooves located at the inner and outer edges of the wall at about 70 and 130 Å, respectively. Similarly, the strong pair of reflections arises from the 10-start family at radii of about 70 and 120 Å, respectively.

The relative positions of the grooves are determined by the phases of the x-ray reflections. From his analysis of electron microscope images of sheets of cytoplasmic tubulin (i.e., parallel arrays of protofilaments), Erickson (6) concluded that the grooves corresponding to the 3-fold, 10-fold, 13-fold, and 26-fold helical lines all intersect in a common origin. We have confirmed these results, and the model shown in Fig. 4 was constructed by combining the electron image phases with the x-ray intensities.

The low resolution model

The microtubule wall may be thought of as consisting of three radial domains. The outside (beyond $r \simeq 115$ Å) shows the dominant protofilament separation, oblique grooves running at 60° to the tubule axis, and an apparent splitting of the subunits (Fig. 4*B*). The central region (between 85 and 115 Å) lacks major density fluctuations. The inside (within $r \simeq 85$ Å) is carved into ridges running at 45°, without obvious subdivisions into protofilaments (Fig. 4*C*). The subunits clearly are not spherical, and their elongated shape near the outer surface gives rise to the unusual intensity distribution on the first layer line. Thus, we have a good picture of the microtubule wall at this resolution, viewed from either the outside or the inside.

We cannot yet fix the shape of an individual tubulin monomer. While the major grooves probably define the boundaries between protein and solvent, we can only define the boundaries between subunits along the vertical grooves separating the protofilaments on the outside. However, the two lobes making up one subunit (Fig. 4*B*) could be combined in several different ways into structure units, some of which would imply the subunit to be 80 Å long axially (6). Moreover, we cannot yet correlate the positions of grooves on the inside and outside. We should point out that the volume contained in a protofilament per 40 Å repeat can accommodate only one tubulin monomer, not an α–β-heterodimer, so that we would rule out the latter as the basic structure unit.

Major intensity on the pattern beyond the area we have discussed is concentrated in a series of three additional layer lines that show strong maxima near the meridian. Their axial repeat is 40.5 ± 0.5 Å. This distribution of intensity signifies that the microtubule wall is further subdivided by grooves along relatively flat helical families. Within the uncertainty produced by the disorientation in these specimens, the positions of these peaks are consistent with the subunit arrangement. Moreover, the radial limits of the wall make it possible to specify which helical families correspond to most of these maxima. Generally, the main helical grooves appear to be located near the inner or outer surfaces of the particle. The intensity of these reflections tells us about the depth of the grooves, but we cannot specify their positions (phases) relative to the other grooves already located on the particle walls.

An additional feature of the pattern is the very weak series of reflections near the meridian midway between the layer lines. These reflections indicate that the microtubule wall has an additional axial repeat of 80 Å, which appears to be a consistent feature of our diagrams from brain and sperm tail microtubules (see ref. 13). Amos and Klug interpreted a strong 80 Å superlattice seen in flagellar microtubules as arising from a pairing of the two similar types of α- and β-tubulin subunits (5). In Erickson's analysis of electron micrographs of brain microtubules (6), he did not detect an 80-Å superlattice and suggested that additional proteins known to be present in flagellar microtubules could be giving rise to some of the large periodicities. Our x-ray analysis indicates that there is some pairing of subunits, but that hydrated α- and β-tubulin monomers appear to have very similar structures. Moreover, the positions of the 80-Å reflections on the x-ray diagrams do not seem compatible with the Amos–Klug superlattice (5) for an intact tubule with 13 protofiliaments (the "A-tubule") (see ref. 15).

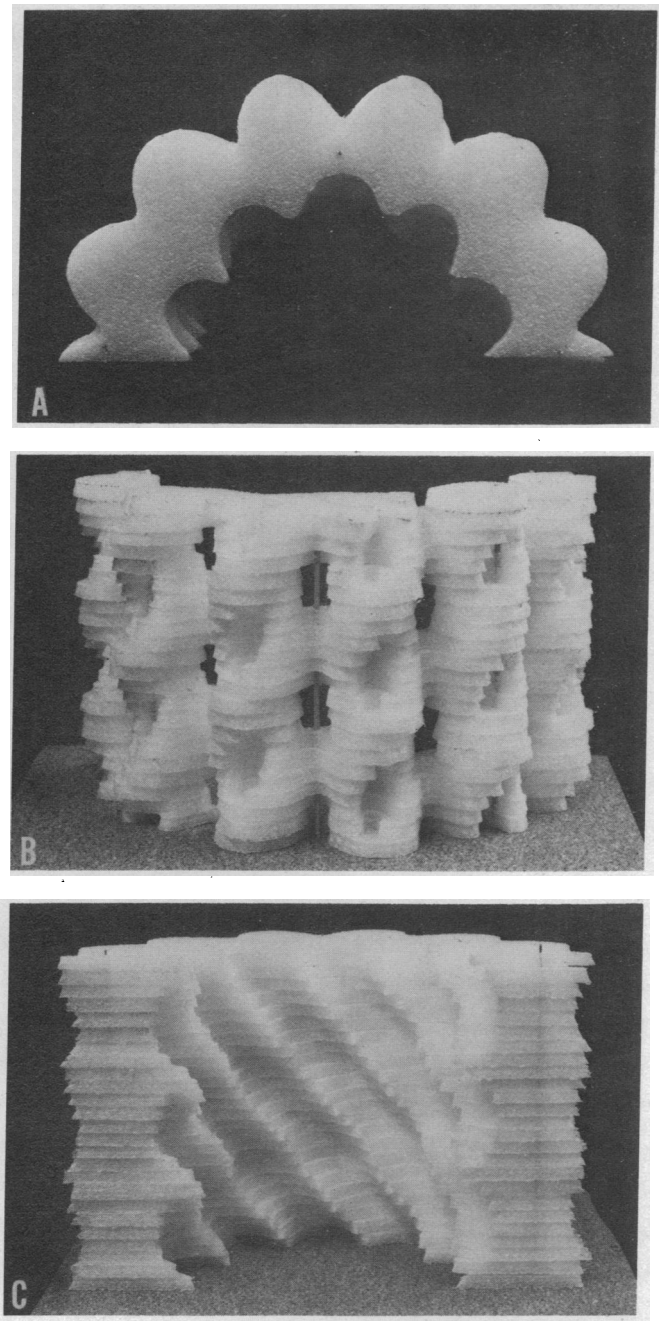

FIG. 4. Model of the microtubule at low resolution. The electron density of the structure was calculated from the x-ray intensities using helical diffraction theory (see ref. 14).

(*A*) View from the top. The microtubule wall extends from 70 Å to 150 Å in radius and is centered at 110 Å. The strong 13-fold density fluctuation at a radius of 126 Å divides the outer wall into protofilaments. A 26-fold fluctuation at a radius of 116 Å deepens these grooves and also produces a slight splitting of the protofilaments, which can be seen in *B*. The inside surface shows a set of 10 ridges that do not reveal the profile of the protofilaments (see also *C*). In this model, a low-density contour was chosen so that one structure unit contains the volume of one tubulin monomer.

(*B*) View from the outside. Choice of a high-density contour (enclosed volume per structure unit only 60% of a tubulin monomer) shows the widening of the grooves and the apparent splitting of the protofilaments. Each subunit appears bilobed, with both halves tilted toward the 10-start helical path. The 3-start density fluctuation at a radius of 133 Å and the 10-start fluctuation at a radius of 119 Å are included as well as those discussed in *A*.

(*C*) View from the inside, low-density contour. The dominant features are the 10-fold grooves inclined at 45°. Note that there appears to be no subdivision into protofilaments on the inside; i.e., the inner tips of the subunits are connected *across* protofilaments. This view includes the 3-start fluctuation at a radius of 68 Å and the 10-start fluctuation at a radius of 70 Å. The models were computed using a common intersection at $\phi = z = 0$ for all grooves.

Conclusions

The early x-ray diffraction diagrams of hydrated microtubules from sperm tail flagella (13) revealed a structure with an overall similarity to that seen in the electron microscope; but there was a puzzling difference in the intensity distribution between the x-ray patterns and optical diffraction patterns of electron micrographs. This was attributed by Cohen *et al.* (13) to a possible difference in the subunit arrangements (surface lattice) in the microtubule gels and the negatively stained preparations used for electron microscopy. They attempted to establish the symmetry of the microtubule surface lattice from these x-ray patterns, but the weak near-meridional reflection (from the 3-start grooves) on the first layer line was obscured. An additional misleading constraint taken from electron microscopy was the value of 120 Å for the outer radius of the microtubule; this restricted the number of possible helical symmetries. We now know that this value is the radius of the deep vertical grooves, which are easily filled with stain, rather than that of the outer tips of the protein subunits. Following the precise description of the surface by Amos and Klug (5), and with the production of more detailed patterns from highly oriented samples of brain microtubules (1), it became apparent that the symmetry proposed by Amos and Klug was probably correct; the intensity differences indicated a difference in apparent subunit shape as seen by these two techniques, rather than a difference in the subunit packing.

We have now shown that most of the contrast in the microtubule particle comes from specific groovings of the microtubule surfaces. The stain penetration in electron microscope preparations appears to strongly enhance the rather shallow family of helices (the 3-start family) on the outside of the wall. The x-ray patterns reveal, however, that under the solvent conditions used (25% glycerol), it is the steep, deeply grooved 10-fold helices and the vertical clefts of the outer wall that describe the alignment of the mass of the protein subunits in the hydrated unstained microtubules. The 3-start family makes only a small contribution, so that the x-ray results show a particle with a subunit appearance different from that derived from electron microscopy. Moreover, the x-ray data reveal that the inner surface of the wall is carved into steep ridges that show little of the protofilament grooving. Further details of the x-ray structure, including a consideration of the subunit pairing and the effect of solvent densities on the appearance of the model, will appear in a forthcoming publication.

We thank Drs. David DeRoisier and Eaton Lattman for discussion, and Drs. Peter Vibert and Walter Phillips for aid in obtaining x-ray photographs. We are indebted to Dr. Eva-Maria Mandelkow for valuable suggestions and for providing electron microscopy data. This work was supported by grants from the U.S. Public Health Service (AM-17346 and GM-21040) and the Max-Planck-Gesellschaft.

1. Cohen, C., DeRosier, D., Harrison, S. C., Stephens, R. E. & Thomas, J., (1975) *Ann. N.Y. Acad. Sci.* **253**, 53–59.
2. Makowski, L. (1976) Doctoral dissertation, Massachusetts Institute of Technology, Cambridge, MA.
3. Weisenberg, R. C. (1972) *Science* **177**, 1104–1105.
4. Shelanski, M. L., Gaskin, F. & Cantor, C. R. (1973) *Proc. Natl. Acad. Sci. USA* **70**, 765–768.
5. Amos, L. A. & Klug, A. J. (1974) *J. Cell Sci.* **14**, 523–549.
6. Erickson, H. P. (1974) *J. Cell Biol.* **60**, 153–167.
7. Ledbetter, M. C. & Porter, K. R. (1964) *Science* **144**, 872–874.

8. Tilney, L. G., Bryan, J., Bush, D. J., Fujiwara, K., Mooseker, M. S., Murphy, D. B. & Snyder, D. H. (1973) *J. Cell Biol.* **59**, 267–275.
9. Linck, R. W. & Amos, L. A. (1974) *J. Cell Sci.* **14**, 551–559.
10. Shelanski, M. L. & Taylor, E. W. (1968) *J. Cell Biol.* **38**, 304–315.
11. Bryan, J. & Wilson, L. (1971) *Proc. Natl. Acad. Sci. USA* **68**, 1762–1766.
12. Olmsted, J. B., Witman, G. B., Carlson, K. & Rosenbaum, J. (1971) *Proc. Natl. Acad. Sci. USA* **68**, 2273–2277.
13. Cohen, C., Harrison, S. C. & Stephens, R. E. (1971) *J. Mol. Biol.* **59**, 375–380.
14. Klug, A., Crick, F. H. C. & Wyckoff, H. W. (1958) *Acta Crystallogr.* **11**, 199–213.
15. Mandelkow, E.-M., Unwin, P. N. T., Mandelkow, E. & Cohen, C. (1977) *Nature*, **265**, 655–657.